Draft version July 10, 2017
Typeset using LaTeX **twocolumn** style in AASTeX61

WATER, HIGH-ALTITUDE CONDENSATES, AND NO METHANE IN THE ATMOSPHERE OF THE WARM NEPTUNE WASP-107b

Laura Kreidberg, Michael Line[1,2]

Michael Line[3]

Caroline Morley[4,5]

Kevin Stevenson[6]

[1] *Harvard Society of Fellows 78 Mt. Auburn St. Cambridge, MA 02138, USA*
[2] *Harvard-Smithsonian Center for Astrophysics 60 Garden St. Cambridge, MA 02138*
[3] *Arizona State University*
[4] *Harvard-Smithsonian Center for Astrophysics*
[5] *Sagan Fellow*
[6] *Space Telescope Science Institute*

Submitted to ApJL

ABSTRACT

WASP-107b is baller.

Keywords: planets and satellites: individual (WASP-107b), planets and satellites: atmospheres

Corresponding author: Laura Kreidberg
laura.kreidberg@cfa.harvard.edu

1. INTRODUCTION

2. OBSERVATIONS

We observed a single transit of WASP-107b with HST's Wide Field Camera 3 (WFC3) instrument on UT 5-6 June 2017. The transit observation consisted of five HST orbits. At the beginning of each 96-minute orbit, we took an image of the target with the F130N filter (exposure time = 4.2 s). This direct image is used for wavelength calibration. For the remainder of the target visibility period (about 45 minutes), we obtained time series spectra with the G141 grism, which provides low-resolution spectroscopy over the wavelength range $1.1 - 1.7\,\mu$m. We used the NSAMP=6, SPARS_25 readout mode (exposure time = 112 s) to optimize the efficiency of the observations, as determined by the `PandExo_HST` planning tool[1]. As is standard for observations of bright targets, we used the spatial scanning observing mode, which smears the spectrum in the spatial direction over the course of an exposure. The scan rate was 0.12 arcseconds/sec.

3. DATA REDUCTION

We reduced the data with the custom pipeline described in Kreidberg et al. (2014), which we summarize briefly here. For each exposure, we extracted the spectrum from each up-the-ramp sample (or "stripe") separately using the optimal extraction algorithm of (Horne 1986). The stripe spectra were then summed to create the final spectrum. For each stripe, the extraction box was 80 pixels high and centered on the stripe's midpoint in the spatial direction. To correct the change in dispersion solution over the length of the spatial scan, we interpolated each row to the wavelength scale of the row corresponding to the spectral trace. We also corrected for slight drift in the spectral direction (< 0.1 pixels) by interpolating each the first exposure. To subtract the background, we took the median of sky pixels that were uncontaminated by the target spectrum (rows $5 - 250$, columns $5 - 15$). The typical background counts were low: 40 photoelectrons/pixel, in comparison to 3×10^4 photoelectrons/pixel in the stellar spectrum.

4. ANALYSIS

The data analysis had two parts: the band-integrated "white" light curve fit and the spectroscopic light curve fits.

4.1. *White Light Curve Fit*

To create the raw white light curve, we summed each spectrum over the 181 pixels in the spectral trace. The white light curve has systematic trends that are typical for WFC3 observations Zhou et al. (2017): the flux increases increases asymptotically over each orbit (the "ramp" effect) and there is a visit-long linear trend. The largest ramp occurs in the initial orbit (orbit zero), so we only fit data from orbits one through four in our analysis, following common practice. We fit the light curve with the analytic model of the form $F_{\rm white}(t) = S_{\rm white}(t) \times T_{\rm white}(t)$, where $S_{\rm white}$ is a systematics model and $T_{\rm white}$ is a transit model. We used the same systematics model as Kreidberg et al. (2015), Equation 1. To model the transit, we used the `batman` package (Kreidberg 2015). The transit model parameters are the orbital period p, time of inferior conjunction t_0, transit depth r_p/r_s, ratio of semi-major axis to stellar radius a/r_s, orbital inclination i, and the quadratic stellar limb darkening parameters u_1 and u_2.

4.1.1. *Star Spot Crossing*

In our initial analysis, we noticed a bump in the light curve during orbit three that could not be fit with our model. We attribute this feature to a star spot crossing event, as WASP-107 is an active star and spot crossings have been observed before (Dai & Winn 2017; Močnik et al. 2017). In our subsequent analysis, we gave the data in orbit three no weight in the fit. The amplitude of the spot crossing feature is FIXME ppm, consistent with a spot of FIXME size and temperature.

4.1.2. *Final Fit*

In our final fit, we fixed the transit parameters a/r_s, i, p on the precise estimates from the Kepler light curve (Dai & Winn 2017). We also fixed the limb darkening parameters on predictions from a PHOENIX model for a star of FIXME properties, calculated with the FIXME package. The remaining free parameters were t_0, r_p/r_s, and the systematics parameters for the visit-long and orbit-long trends.

For the best fit light curve, the root-mean-square residuals were FIXME ppm (not including orbit three), somewhat larger than the expected shot noise of FIXME ppm. The achieved rms is close to the best value obtained for WFC3 data (FIXME), and we attribute the slight excess noise to either additional star spot crossings or loss of flux from the edge of the detector (as has been seen for other bright targets; **?**). We used the Markov chain Monte Carlo algorithm to estimate parameter uncertainties (as implemented in the the `emcee` package; FIXME). We scaled the per-point uncertainties by a factor of FIXME to achieve a reduced χ_2 value of

[1] https://github.com/spacetelescope/PandExo_HST

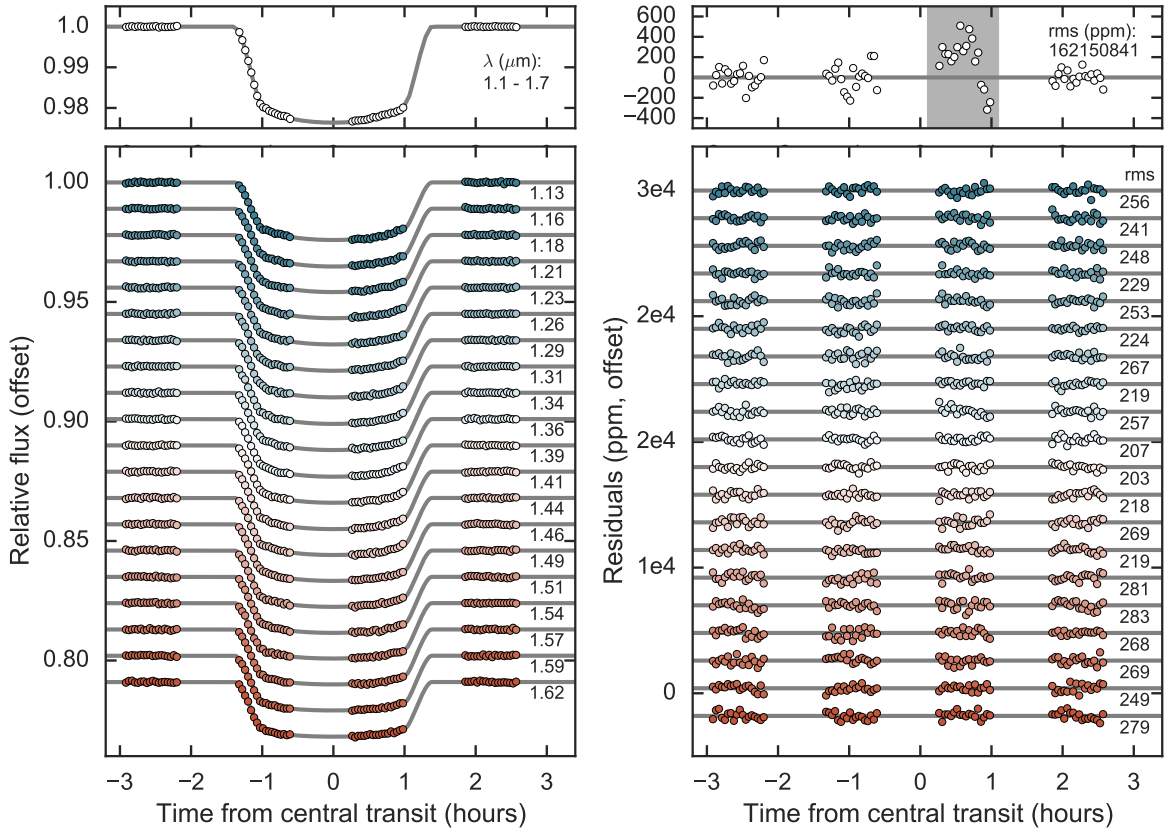

Figure 1. FIXME

unity. The transit time was FIXME and the planet/star radius was FIXME.

4.2. *Spectroscopic Light Curve Fits*

We binned the spectrum into 20 spectrophotometric channels from FIXME to FIXME μm, shown in Figure FIXME. We fit the light curves with the `divide-white` technique, which assumes that the light curve systematics are nearly constant as a function of wavelength (**?**Kreidberg et al. 2014). For this method, the transit model $T_\lambda(t)$ is multiplied by the systematics vector from the white light curve fit ($F_{\rm white}/T_{\rm white}$), and rescaled by a factor $C_\lambda + V_\lambda t$. An advantage of this approach is that it removes the star spot crossing feature, enabling us to use orbit three with no additional correction. There is a small chromatic effect due to the changing amplitude of the spot crossing feature with wavelength, but this effect is below the level of noise in our data FIXME. As for the white light curve, we fixed some of the transit parameters on the estimates from Dai & Winn (2017) and fixed the limb darkening on the PHOENIX model. The fit has just three free parameters: C_λ, V_λ, and r_p/r_s.

The best fit light curves have a median reduced χ_2 value of FIXME and rms values consistent with the expected photon shot noise. There are two channels with slightly higher χ_2 values: FIXME and FIXME. We therefore rescale the photometric uncertainties for all spectroscopic channels such that the χ_2 values are unity, to ensure that we do not underestimate the uncertainty on the transit depths. We performed an MCMC fit to the light curves with `emcee`. The median transit depths and $1\,\sigma$ uncertainties are given in Table FIXME. FIXME: does the median agree with the best fit? FIXME: convergence?

We explored several alternative choices for the spectroscopic light curve fits, but found that none of them made a significant difference in the transmission spectrum. We tested fitting the spectroscopic light curves with the same analytic model we used for the white light curve and obtained nearly identical relative transit depths (FIXME sigma), except offset by a constant value of FIXME ppm. We attribute the offset to the uncorrected star-spot crossing feature. Regardless of the cause, the offset does not affect our final analysis, be-

cause the planet's 1 bar radius is a free parameter in the atmospheric retrieval (see §FIXME). We also explored fitting for a linear limb darkening parameter rather than fixing the limb darkening on the PHOENIX model predictions, and found that the 'fitted limb darkening coefficients are consistent with the model. We opted to fix the coefficients in our final analysis because the uncertainties on the transit depths are slightly smaller (about 10%). We also checked whether the uncertainty in the stellar parameters significantly affects the PHOENIX model predictions, and found that changing the stellar

4.2.1. *Transit Depths Redder than FIXME μm*

The red edge of the transmission spectrum is of interest for our analysis because methane becomes the dominant absorber over water at wavelengths $> 1.6\,\mu$m. Unfortunately, we find that the spectroscopic light curves between FIXME μm are too poor in quality to accurately measure the transit depth. The residuals show evidence for correlated noise and the reduced χ_2 values increase to FIXME.

4.3. *Independent Analysis*

We also performed an independent data reduction and fit using K. Stevenson's pipeline.

5. ATMOSPHERIC RETRIEVAL

We use the CHIMERA chemically-consistent transmission retrieval tool described in Kreidberg et al. (2015) to determine the basic atmospheric properties. Briefly, the transmission spectrum solves the transmission geometry problem using the equations in Brown (2001); Tinetti et al. (2012). We parametrize atmospheric composition with metallicity and carbon-to-oxygen ratio (C/O) under the assumption of thermochemical equilibrium using the NASA CEA routine (**?**) to compute the molecular abundances for H_2, He, H_2O, CH_4, CO, CO_2, NH_3, H_2S, Na, K, HCN, C_2H_2, TiO, VO, and FeH. We have subsequently upgraded the transmission model to use correlated-K opacities (Lacis & Oinas 1991; Mollière et al. 2015; Amundsen et al. 2016) for the aforementioned gases generated from the pretabulated line-by-line cross section database (dv/v 10^6) described in Freedman et al. (2014). The transmission forward model is coupled with the powerful PyMultiNest tool (Buchner 2016) to solve the parameter estimation and model selection problems.

The nominal model set-up requires a temperature-pressure profile (parameterized via the Guillot 2010 relations), the atmospheric metallicity and carbon-to-oxygen ratio for molecular composition determination, disquilibrium properties crudely parameterized with nitrogen species and carbon species quench pressures (Morley et al. 2017), and aerosol properties. We experiment with three atmospheric scenarios within this setup (Table XX): Scenarios with and without methane, and with/without patchy cloud cover (as described and implemented in Line et al. 2016. In all three scenarios we fix the T-P profile "shape" but scale the irradiation temperature, which incorporates unknown variables like the albedo and heat transport efficiency. T-P profile shape information is not readily retrievable, nor does it strongly influence information derived from WFC3 transmission spectra (e.g. Kreidberg et al. 2015). We also switch off the quench pressure parameters as they are unlikely to strongly influence the equilibrium abundance profiles of the spectrally prominent, nearly constant-with-altitude abundance, species like CH_4, H_2O, and NH_3 over this temperature range (e.g. Line et al. 2011; Moses et al. 2013). Aerosols are simply parameterized with a "gray cloud top pressure" with the option for cloud patchiness. We do not consider "sloped hazes" at this time as they are unlikely to influence the results.

6. DISCUSSION

6.1. *Methane*

6.2. *Comparative planetology with HAT-P-11b, HAT-P-26b*

6.3. *Constraints on Condensate Properties*

The amplitude of WASP-107b's spectral features is about half that expected for an atmosphere free of condensates. In our retrieval analysis, we explored two simple parameterizations to model condensates: a gray opacity source and a sloped haze. The retrieved cloud-top pressure is FIXME at $1\,\sigma$ confidence.

We also considered physically motivated, self-consistent cloud and haze models based on . To model WASP-107b's spectrum with self-consistent aerosols, we use the methods described in (Fortney et al. 2008; Morley et al. 2015). We include models from solar to $50\times$ solar metallicity and solar C/O ratio. We model clouds that form in cool atmospheres (Na_2S, KCl, ZnS, see Morley et al. 2012), varying the cloud sedimentation efficiency from 0.1 to 3. None of the cloudy models are sufficiently low amplitude to match the observed muted signal. We also model an ad hoc photochemical 'soot' layer near the top of the atmosphere, scaling results from previous photochemical models for GJ 436b (Line et al. 2011; Morley et al. 2017). With a sufficiently thick photochemical haze with particle sizes around $0.03 - 0.1$ microns, the amplitude of the model water feature matches that of the observations.

6.4. *Atmospheric Metallicity Predictions from Interior Structure Modeling*

7. FUTURE PLANS

Combine data from Spitzer/HST JWST GTO

Fei Dai Jessica Spake

L.R.K. acknowledges support from the Harvard Society of Fellows and the Harvard Astronomy Department Institute for Theory and Computation.

Facilities: HST(WFC3)

REFERENCES

Amundsen, D. S., Mayne, N. J., Baraffe, I., et al. 2016, A&A, 595, A36

Brown, T. M. 2001, ApJ, 553, 1006

Buchner, J. 2016, PyMultiNest: Python interface for MultiNest, Astrophysics Source Code Library, , , ascl:1606.005

Dai, F., & Winn, J. N. 2017, AJ, 153, 205

Fortney, J. J., Lodders, K., Marley, M. S., & Freedman, R. S. 2008, ApJ, 678, 1419

Freedman, R. S., Lustig-Yaeger, J., Fortney, J. J., et al. 2014, ApJS, 214, 25

Guillot, T. 2010, A&A, 520, A27

Horne, K. 1986, PASP, 98, 609

Kreidberg, L. 2015, PASP, 127, 1161

Kreidberg, L., Bean, J. L., Désert, J.-M., et al. 2014, Nature, 505, 69

Kreidberg, L., Line, M. R., Bean, J. L., et al. 2015, ApJ, 814, 66

Lacis, A. A., & Oinas, V. 1991, J. Geophys. Res., 96, 9027

Line, M. R., Vasisht, G., Chen, P., Angerhausen, D., & Yung, Y. L. 2011, ApJ, 738, 32

Line, M. R., Stevenson, K. B., Bean, J., et al. 2016, AJ, 152, 203

Mollière, P., van Boekel, R., Dullemond, C., Henning, T., & Mordasini, C. 2015, ApJ, 813, 47

Morley, C. V., Fortney, J. J., Marley, M. S., et al. 2012, ApJ, 756, 172

—. 2015, ApJ, 815, 110

Morley, C. V., Knutson, H., Line, M., et al. 2017, AJ, 153, 86

Moses, J. I., Madhusudhan, N., Visscher, C., & Freedman, R. S. 2013, ApJ, 763, 25

Močnik, T., Hellier, C., Anderson, D. R., Clark, B. J. M., & Southworth, J. 2017, MNRAS, 469, 1622

Tinetti, G., Tennyson, J., Griffith, C. A., & Waldmann, I. 2012, Philosophical Transactions of the Royal Society of London Series A, 370, 2749

Zhou, Y., Apai, D., Lew, B. W. P., & Schneider, G. 2017, AJ, 153, 243